Article

# Direct evidence for a carbon–carbon one-electron σ-bond

https://doi.org/10.1038/s41586-024-07965-1

Received: 24 November 2023

Accepted: 20 August 2024

Published online: 25 September 2024

Check for updates

Takuya Shimajiri[1,2,3]✉, Soki Kawaguchi[1], Takanori Suzuki[1] & Yusuke Ishigaki[1]✉

Covalent bonds share electron pairs between two atoms and make up the skeletons of most organic compounds in single, double and triple bonds. In contrast, examples of one-electron bonds remain scarce, most probably due to their intrinsic weakness[1–4]. Although several pioneering studies have reported one-electron bonds between heteroatoms, direct evidence for one-electron bonds between carbon atoms remains elusive. Here we report the isolation of a compound with a one-electron σ-bond between carbon atoms by means of the one-electron oxidation of a hydrocarbon with an elongated C–C single bond[5,6]. The presence of the C•C one-electron σ-bond (2.921(3) Å at 100 K) was confirmed experimentally by single-crystal X-ray diffraction analysis and Raman spectroscopy, and theoretically by density functional theory calculations. The results of this paper unequivocally demonstrate the existence of a C•C one-electron σ-bond, which was postulated nearly a century ago[7], and can thus be expected to pave the way for further development in different areas of chemistry by probing the boundary between bonded and non-bonded states.

Unlocking the nature of covalent bonds is important to gain a deeper understanding of chemical phenomena. The concept of two atoms sharing an electron pair, which was initially proposed by Lewis in 1916 (ref. 8) and then termed 'covalent bond' in 1919 by Langmuir[9], remains relevant in understanding chemical bonding.

Subsequently, Pauling proposed a concept of covalent bonds with one unpaired electron ('one-electron σ-bonds'), which is shared between two atoms[7]. In 1931, Pauling postulated the existence of one-electron σ-bonds using the $H_2^{\bullet+}$ radical cation as a simple model. Such one-electron σ-bonds are expected to be much weaker than typical two-electron σ-bonds and, therefore, their properties have been investigated primarily theoretically[10–13]. Nevertheless, few studies on in situ generated radical anions[14–17] such as $R_3B{\bullet}BR_3^-$ and radical cations[10,18–20] such as $R_3E{\bullet}ER_3^+$ (E = C, Si and Ge) based on electron spin resonance measurements have been reported. Other reports have described the spectroscopic identification of chemical species with one-electron σ-bonds that were generated as single components; however, these compounds have not been isolated[21,22]. X-ray crystallographic studies on species that contain one-electron σ-bonds are particularly scarce, that is, they are limited to P•P, B•B and Cu•M (M = B, Al and Ga) bonds[1–4]. It is important to note here that, although species with C•C one-electron σ-bonds have been proposed as intermediates in chemical reactions such as the Cope rearrangement, there is no experimental evidence by, for example, X-ray crystallography for one-electron σ-bonds between carbon atoms[23–28].

## Synthesis and characterization of $1^{\bullet+}$

$R_3C{\bullet}CR_3^+$ radical cations are promising models with which to investigate C•C one-electron σ-bonds[18,20]. However, reports on molecules that contain a C•C one-electron σ-bond remain elusive at present due to their intrinsically high reactivity, and stabilizing such compounds is as important a task as it is challenging. One approach to circumvent this obstacle is to use hexaphenylethane (HPE) derivatives, which can be expected to provide a suitable framework because their oxidation would lead to the formation of triarylmethyl cation and triarylmethyl radical units, which are well known, relatively stable, carbocations and radicals.

An important issue in this context is that most redox-active HPEs undergo a process close to a one-step two-electron oxidation to produce two triarylmethyl cations because the oxidation potential for the bond-dissociated radical, which is generated readily by the C–C bond scission of the radical cation intermediate, is much less positive than that for neutral σ-bonded species ($E_1^{ox} > E_2^{ox}$) (Fig. 1, top). To obtain a radical cation with a C•C one-electron σ-bond, the oxidation of HPEs must proceed in a stepwise manner, that is, the level of the highest occupied molecular orbital (HOMO) for the neutral state must be higher than that of the singly occupied molecular orbital (SOMO) for the radical cation ($E_1^{ox} < E_2^{ox}$). Although raising the HOMO level is considered to be essential, the introduction of electron-donating heteroatoms into HPEs is not effective because it simultaneously raises the HOMO level of the neutral species and the SOMO level of the radical cations. Thus, alternative approaches for achieving a stepwise oxidation process are required.

We tackled this issue by focusing on another notable feature of HPEs, which is that the central C–C single bond is elongated beyond 1.6 Å due to the steric hindrance imposed by the aryl groups surrounding the bond[29–33]. This bond elongation causes an increase in the HOMO level by means of a through-bond interaction between the elongated C–C bond and the aryl groups. Thus, the bond elongation in HPEs provides an optimal approach to realize an energy reversal between the HOMO of the neutral state and the SOMO of the radical cation state without

[1]Department of Chemistry, Faculty of Science, Hokkaido University, Sapporo, Japan. [2]Creative Research Institution, Hokkaido University, Sapporo, Japan. [3]Present address: Department of Chemistry, Graduate School of Science, The University of Tokyo, Tokyo, Japan. ✉e-mail: shimajiri@chem.s.u-tokyo.ac.jp; yishigaki@sci.hokudai.ac.jp

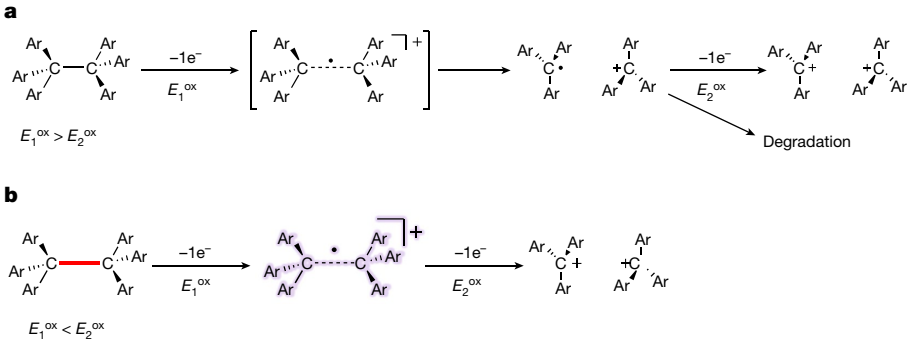


**Fig. 1 | Proposed redox mechanisms in HPE derivatives. a**, Typical oxidation processes in HPEs. **b**, Oxidation in the HPE derivative with an ultralong C–C single bond.

relying on the introduction of electron-donating heteroatoms (Fig. 1, bottom).

HPE **1** (refs. 5,6) bears two spiro-dibenzocycloheptatriene (DBCHT) units and thus satisfies the aforementioned key factors, that is, it has an extremely elongated C$sp^3$–C$sp^3$ single bond (1.806(2) Å at 400 K), which is the highest value among hitherto reported HPEs. Such an extremely elongated C–C bond increases the HOMO level by means of a through-bond interaction, resulting in a stepwise oxidation process ($E_{1/2}^{ox1}$ = +0.57 V and $E_{1/2}^{ox2}$ = +0.69 V versus saturated calomel electrode) that was observed by cyclic voltammetry[34]. Furthermore, the rigid acenaphthylene core causes a bond elongation in the neutral-state C…C distance required to form a one-electron bond. The naphthalene core, on the other hand, is not suitable to cause the stepwise oxidation in the corresponding hydrocarbon, although that worked well in the case of the B•B one-electron bond reported in ref. 21. We predicted that HPE **1** could potentially serve as a suitable platform to stabilize the C•C one-electron σ-bond through an intramolecular core–shell strategy.

Figure 2a shows the redox reactions of **1**. A two-electron oxidation was achieved by treating **1** with iodine (3.0 equiv.) to furnish dication salt $\mathbf{1}^{2+}(I_3^-)_2$, of which single crystals were obtained after recrystallization from $CH_2Cl_2$/diethyl ether. Meanwhile, the one-electron oxidation of **1** with iodine (1.5 equiv.) provided $\mathbf{1}^{\bullet+}I_3^-$ as a dark brown solid that is sparingly soluble in organic solvents such as $CH_2Cl_2$ and acetonitrile. The formation of paramagnetic species was confirmed by the absence of any $^1$H nuclear magnetic resonance (NMR) signals and the presence of a characteristic doublet electron spin resonance signal in solution. Recrystallization of the radical cation salt $\mathbf{1}^{\bullet+}I_3^-$ from acetonitrile/diethyl ether afforded dark violet single crystals suitable for X-ray diffraction measurements. Upon reduction of the cationic species with zinc powder, the original compound **1** was restored.

## X-ray analysis

The single crystals obtained were subjected to an X-ray diffraction analysis to explain redox-state-dependent differences in the molecular structures. The X-ray structure of dication $\mathbf{1}^{2+}$ in $\mathbf{1}^{2+}(I_3^-)_2$ exhibits a twisted conformation with a twisting C1–C3–C4–C2 angle ($\theta$) of 20.8(6)°, while both DBCHT moieties are planar (Fig. 2c). As in the case of $\mathbf{1}^{2+}(I_3^-)_2$, typical dibenzocycloheptatrienylium (cation) and dibenzocycloheptatrienyl (radical) derivatives would be expected to exhibit a preference for planarity, which is more conducive to π-stacking and electron delocalization[35–37]. In contrast, an eclipsed conformation with a small $\theta$ value of 2.19(19)° was observed in the X-ray structure of $\mathbf{1}^{\bullet+}$ in $\mathbf{1}^{\bullet+}I_3^-$ (Fig. 2d,e). One of the DBCHT moieties in $\mathbf{1}^{\bullet+}$, that is, the one containing C1, adopts a bent geometry with larger dihedral angles between the *a*–*e* planes (Fig. 2). The concave surface of the bent seven-membered ring faces the other DBCHT unit, that is, the one containing C2, which exhibits an almost planar geometry. The estimated s.d. of the structural parameters (bond length: 0.004 Å; bond angle: 0.3°) and R indices (R1 = 0.0220; wR2 = 0.0569) for $\mathbf{1}^{\bullet+}I_3^-$ were sufficiently small to confirm the unsymmetrical bent-planar structure, and the nearly perfect round shape of the thermal ellipsoids of C1 and C2 excludes the possibility of a disordering copresence of **1** or $\mathbf{1}^{2+}$ at the site of $\mathbf{1}^{\bullet+}$. Crystals of $\mathbf{1}^{\bullet+}I_3^-$ can be stored under ambient conditions for at least two weeks without appreciable decomposition and remained intact even during high-temperature X-ray measurements at 400 K (Supplementary Fig. 4). The observed geometrical difference between $\mathbf{1}^{\bullet+}$ and $\mathbf{1}^{2+}$ is intrinsic and reproducible, which was confirmed by analysing several single crystals of $\mathbf{1}^{\bullet+}I_3^-$ and $\mathbf{1}^{2+}(I_3^-)_2$.

This distinctive geometry deviates from the typical planar conformation of a pimer composed of cationic and radical moieties/molecules[38–40]. Contrary to the unsymmetric structure of $\mathbf{1}^{\bullet+}I_3^-$, the bond lengths in the two different DBCHT moieties are almost identical (Supplementary Tables 1 and 2), which indicates that the spin and positive charge are delocalized over the two DBCHT moieties in $\mathbf{1}^{\bullet+}I_3^-$, that is, spin and charge-separated states are not favoured. Other effects between the two DBCHT moieties stem most probably from the stabilization of the unique and unsymmetric bent conformation. At present, we consider that the molecular structure of $\mathbf{1}^{\bullet+}$ with an unsymmetric bent-planar geometry is similar to that of **1**, which implies an inheritance from the covalent bond nature between the C1 and C2 atoms. In fact, the short contact between the C1 and C2 atoms (2.921(3) Å at 100 K) was confirmed in the X-ray structure of $\mathbf{1}^{\bullet+}I_3^-$ (Fig. 2e). The sum of the three bond angles around the C1 (359.3°) and C2 (359.6°) atoms indicates that each atom is $sp^2$ hybridized despite the unsymmetrical bent-planar geometry. This finding is consistent with previous examples of weak C…C bondings, in which the carbon atoms involved exhibit a preference for $sp^2$ hybridization[41,42]. Focusing on the intramolecular C…C distance between the two DBCHT units, although some interatomic distances (2.92–3.32 Å) closer to the naphthalene skeleton were found to be less than the sum of the van der Waals radii of carbon atoms (3.40 Å), most are greater (3.44–3.79 Å), indicating an unfavourable conformation for stabilization by π–π interactions (Supplementary Fig. 10 and Supplementary Table 1). This behaviour contrasts with the usual planar π-systems, indicating that stabilizing interactions other than π–π stacking are occurring between the DBCHT units. In the crystal, short intermolecular contacts between one DBCHT unit and $I_3^-$ (approximately 3.5 Å; sum of the van der Waals radii: 3.8 Å) were observed. However, they correspond to the proximity of the σ-hole—a positively polarized site—in the $I_3^-$ ion and the cationic π-surface of DBCHT and, accordingly, this intermolecular interaction has little effect on the geometrical features of $\mathbf{1}^{\bullet+}$ in crystal. It is also worth noting here that residual electron density between the C1 and C2 atoms is present in the Fo–Fc map that was obtained from the X-ray analysis of $\mathbf{1}^{\bullet+}I_3^-$ (Fig. 3a–c), which proves electron sharing between the C1 and C2 atoms. This electron sharing contributes to the molecular stability, which predestines radical cation $\mathbf{1}^{\bullet+}$ to serve as a host for a

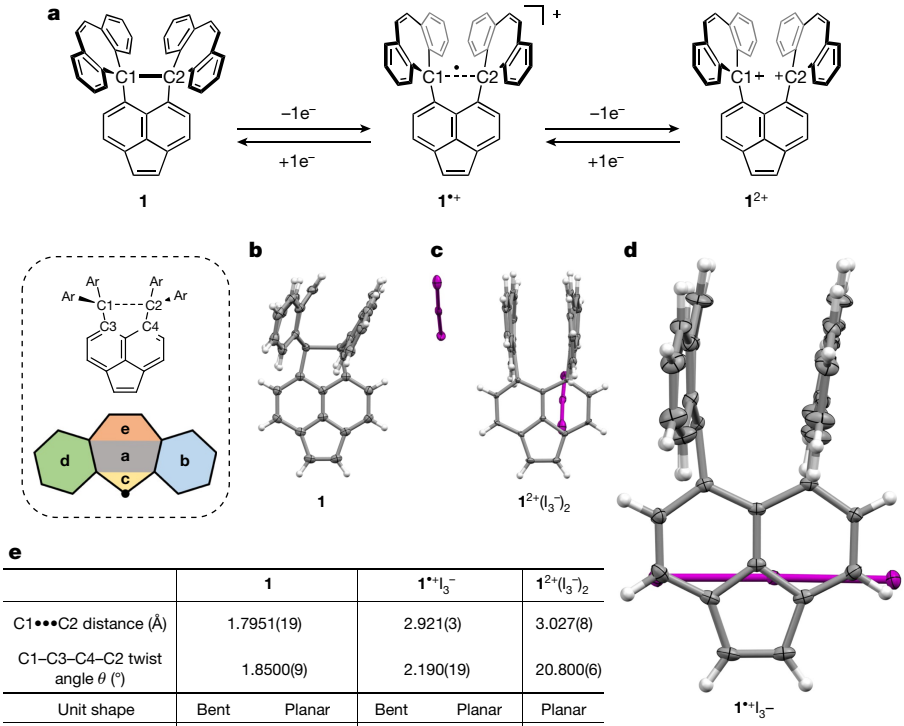


**e**

| | | 1 | | $1^{\bullet+}I_3^-$ | | $1^{2+}(I_3^-)_2$ |
|---|---|---|---|---|---|---|
| C1•••C2 distance (Å) | | 1.7951(19) | | 2.921(3) | | 3.027(8) |
| C1–C3–C4–C2 twist angle $\theta$ (°) | | 1.8500(9) | | 2.190(19) | | 20.800(6) |
| Unit shape | | Bent | Planar | Bent | Planar | Planar |
| Dihedral angle (°) | a–b | 24.74(5) | 7.77(5) | 11.09(9) | 1.83(10) | 2.33(16) |
| | a–c | 49.80(13) | 13.99(15) | 15.80(3) | 4.00(3) | 7.90(6) |
| | a–d | 24.17(5) | 3.81(5) | 8.87(9) | 2.43(10) | 5.93(17) |
| | a–e | 24.32(11) | 2.93(11) | 11.30(2) | 1.38(18) | 7.50(4) |

Standard C$sp^3$–C$sp^3$ single bond length: 1.54 Å
Sum of the van der Waals radii of carbon atoms: 3.4 Å

**Fig. 2 | Redox reactions and X-ray structures. a**, Redox interconversion of **1**. **b**–**d**, X-ray structures of **1** (**b**) and $\mathbf{1}^{\bullet+}I_3^-$ (**d**) at 100 K and $\mathbf{1}^{2+}(I_3^-)_2$ (**c**) at 110 K with thermal ellipsoids at 50% probability. **e**, Structural parameters determined at 100 K for **1** and $\mathbf{1}^{2+}(I_3^-)_2$ and at 110 K for $\mathbf{1}^{\bullet+}I_3^-$. Due to the phase transition occurring at around 100 K, the X-ray analysis of $\mathbf{1}^{2+}(I_3^-)_2$ was conducted at 110 K; disordered $I_3^-$ is omitted for clarity in $\mathbf{1}^{2+}(I_3^-)_2$.

C•C one-electron σ-bond with a bond length of 2.921(3) Å. In the case of the B•B one-electron bond, which is based on the naphthalene core, a similar interatomic distance was predicted[21], whereas a smaller value was determined in the corresponding molecule with a biphenyl core. This difference should most probably be interpreted in terms of the rigidity of the π-framework.

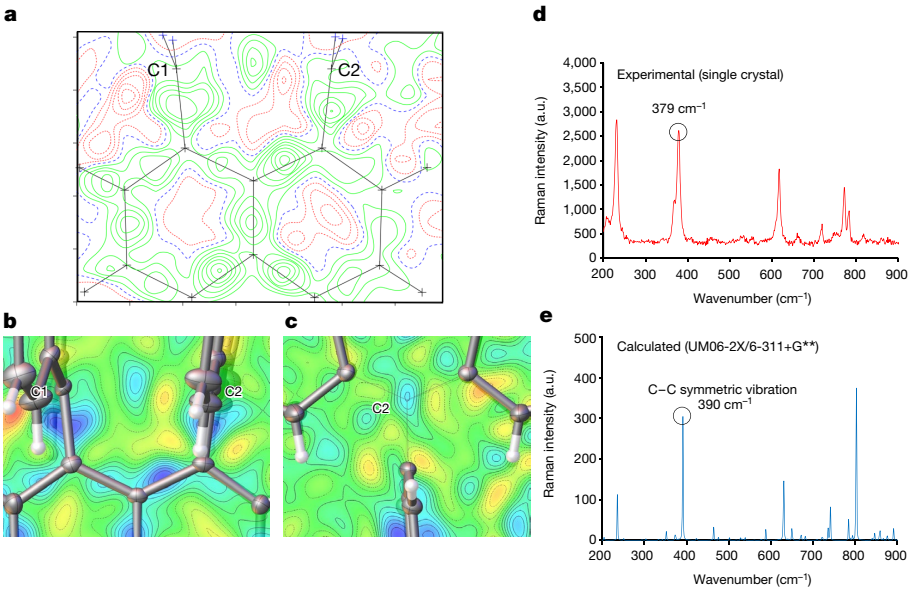


**Fig. 3 | Experimental evidence of the presence of a C•C one-electron σ-bond in $\mathbf{1}^{\bullet+}(I_3^-)$. a**–**c**, Experimentally obtained Fo–Fc maps of $\mathbf{1}^{\bullet+}I_3^-$ at 100 K on the C1–C3–C4–C2 plane (**a**,**b**) and on its orthogonal plane (**c**) through the midpoint between the C1 and C2 atoms (C2 → C1 direction). Residual electron density is shown in green (**a**) and blue (**b**,**c**). **d**, Raman spectrum measured at 298 K using a single crystal of $\mathbf{1}^{\bullet+}I_3^-$. **e**, Simulated Raman spectrum for $\mathbf{1}^{\bullet+}$ obtained from DFT calculations at the UM06-2X/6-311+G** level.

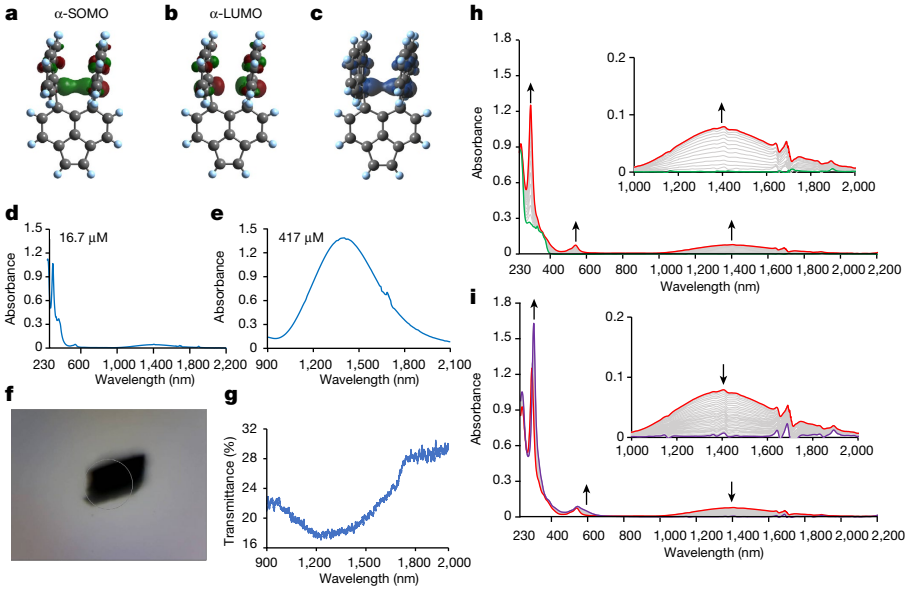


**Fig. 4 | Electronic properties of $1^{\bullet+}$ with a C•C one-electron σ-bond. a**–**c**, Kohn–Sham orbitals of the α-SOMO (**a**), the α-LUMO (isovalue = 0.05) (**b**), and spin density (isovalue = 0.004) (**c**) obtained from DFT calculations at the UM06-2X/6-311+G** level. The atomic coordinates of the X-ray structure of $\mathbf{1}^{\bullet+}I_3^-$ at 100 K were used for the calculations. **d**,**e**,**g**, UV/Vis/NIR absorption spectra in $CH_2Cl_2$ (**d**, 16.7 μM; **e**, 417 μM) and for a single crystal of $\mathbf{1}^{\bullet+}I_3^-$ (**g**). **f**, Photograph of a single crystal of $\mathbf{1}^{\bullet+}I_3^-$. **h**,**i**, Changes (black arrows) in UV/Vis/NIR spectra upon constant-current electrochemical oxidation of **1** (11.1 μM, 30 μA, every 2 min) in $CH_2Cl_2$ containing 0.05 M $Bu_4NBF_4$ as a supporting electrolyte: first step (0–28 min, **1** to $\mathbf{1}^{\bullet+}$) (**h**); second step (28–90 min, $\mathbf{1}^{\bullet+}$ to $\mathbf{1}^{2+}$) (**i**).

## Experimental and theoretical analyses

To verify whether this electron sharing corresponds to the bond, a single crystal of $\mathbf{1}^{\bullet+}I_3^-$ was subjected to Raman spectroscopy at 298 K to obtain direct information about the force constant of the bond. The experimentally obtained and simulated Raman spectra of $\mathbf{1}^{\bullet+}$ are shown in Fig. 3d,e. The simulated spectrum obtained from density functional theory (DFT) calculations at the UM06-2X/6-311+G** level accurately reproduced the experimental results. The observed Raman shift ($\mathbf{1}^{\bullet+}I_3^-$: 379 $cm^{-1}$) attributed to the symmetric C1–C2 stretching vibration is significantly lower than that for neutral **1**, which contains an ultralong C–C single bond (589 $cm^{-1}$)[5,6]. However, this Raman shift is higher than that observed in molecules that contain C…C bonding interactions beyond 2.0 Å (refs. 41,42). This contrasts with the common absence of Raman shifts for weak interactions in π-stacked molecules such as pimers.

Next, DFT calculations were carried out to obtain more information on the strength of the C•C one-electron σ-bond. The estimated force constant for $\mathbf{1}^{\bullet+}$ (56.8 N $m^{-1}$), which was obtained as a second derivative of the energy with respect to the bond length at the (U)M06-2X/6-31+G** level based on the Lennard–Jones potential, is much smaller than that for **1** (113.7 N $m^{-1}$) or ethane (445.9 N $m^{-1}$). The estimated force constant is in good agreement with the calculated value (50.8 N $m^{-1}$) obtained from the relationship between the force constant and the vibrational frequency using the value of the observed Raman shift of the symmetric C1–C2 stretching vibration (for details, see Supplementary Information). These results indicate a covalent nature of the electron sharing between the C1 and C2 atoms in $\mathbf{1}^{\bullet+}I_3^-$.

Le Floch et al. reported that the radical anion of the calixarene exhibits a short C…C distance (3.323(3) Å)[43]. From a theoretical point of view, the coefficients of the SOMO indicate that a bonding orbital between the carbon atoms in close proximity was not formed since they reside on the nodal plane. Thus, a detailed investigation is needed to verify whether this short contact represents a bond or is due merely to physical proximity. To gain further insight into the electronic structure, DFT calculations for $\mathbf{1}^{\bullet+}$ were performed at the UM06-2X/6-311+G** level based on the X-ray coordinates. The results indicate that the SOMO, the lowest unoccupied molecular orbital (LUMO) and the spin density are located mainly on the C1 and C2 atoms (Fig. 4a–c). According to the shape of the orbitals, the α-SOMO and α-LUMO of $\mathbf{1}^{\bullet+}$ represent the σ-type bonding and σ*-type antibonding orbitals, respectively. In the natural bond orbital (NBO) analysis of $\mathbf{1}^{\bullet+}$, both orbitals were confirmed for the C1 and C2 atoms as well. The C1–C2 bond exhibits 0.3–0.4% 2*s* character and 99.6–99.7% 2*p* character, with 0.76 electrons involved in the bond. Equal values of a positive charge for both C1 (0.05) and C2 (0.05) atoms in $\mathbf{1}^{\bullet+}$ were estimated using natural population analysis methods, indicating a delocalized charge distribution in the DBCHT moieties. The natural population analysis also predicted a relatively large spin-density distribution on the C1 (0.26) and C2 (0.24) atoms. A localized molecular orbital analysis using the Foster–Boys method showed that the contribution of the C1 (28.0%) and C2 (27.5%) atoms in the α-SOMO is dominant and that the contributions of the other atoms is less than 5%. The shape of the localized α-SOMO clearly reflects the formation of the σ-orbital (Supplementary Fig. 21). Considering these results and the comparable bond lengths in each DBCHT moiety, the contribution of a coordinating-type bonding interaction can be excluded, that is, these results indicate that a σ-bond between carbon atoms could be maintained even if fewer than one electron is involved. Furthermore, we carried out bond topological analyses including quantum theory of atom in molecules and electron localized functions for the whole series. Each parameter for $\mathbf{1}^{\bullet+}$ exhibits an intermediate value between those of bonded **1** and non-bonded $\mathbf{1}^{2+}$, which indicates that $\mathbf{1}^{\bullet+}$ possesses an intermediary nature. This finding is consistent with the notion of the presence of a one-electron bond, which would be expected to fall between a two-electron bond and a non-bonded state.

In their entirety, the experimental and theoretical results indicate that the short C1…C2 contact with a value of 2.921(3) Å in $\mathbf{1}^{\bullet+}I_3^-$ is, although weak, an example of a C•C one-electron σ-bond.

To investigate the properties of the compound from the photochemical point of view, we recorded the ultra-violet/visible/near-infrared (UV/Vis/NIR) spectrum of $\mathbf{1}^{\bullet+}I_3^-$ in $CH_2Cl_2$. An NIR absorption band was observed at around 2,000 nm ($\lambda_{max} \simeq 1{,}405$ nm) (Fig. 4d,e), which cannot be explained by disproportionation ($2 \times \mathbf{1}^{\bullet+} \rightleftarrows \mathbf{1} + \mathbf{1}^{2+}$) because neither **1** nor $\mathbf{1}^{2+}$ exhibits such an NIR absorption (Fig. 4h,i and

Supplementary Fig. 15). In solution, $\mathbf{1}^{\bullet+}$ could exist in an equilibrium between the σ-bonded form and the pimer-like form predicted by DFT calculations (for details, see Supplementary Information). To confirm that the pimer-like form is not responsible for the NIR absorption, a solid-state absorption spectrum was recorded using a single crystal of $\mathbf{1}^{\bullet+}\mathbf{I}_3^-$, which showed an NIR absorption in the same region as that in solution (Fig. 4f,g). Thus, the NIR absorption for $\mathbf{1}^{\bullet+}\mathbf{I}_3^-$ can be attributed to the σ–σ* transition of the weak C•C one-electron bond.

## Online content

Any methods, additional references, Nature Portfolio reporting summaries, source data, extended data, supplementary information, acknowledgements, peer review information; details of author contributions and competing interests; and statements of data and code availability are available at https://doi.org/10.1038/s41586-024-07965-1.


1. Canac, Y. et al. Isolation of a benzene valence isomer with one-electron phosphorus-phosphorus bonds. *Science* **279**, 2080–2082 (1998).
2. Moret, M., Zhang, L. & Peters, J. C. A polar copper–boron one-electron σ-bond. *J. Am. Chem. Soc.* **135**, 3792–3795 (2013).
3. Hübner, A. et al. Confirmed by X-ray crystallography: the B·B one-electron σ bond. *Angew. Chem. Int. Ed.* **53**, 4832–4835 (2014).
4. Graziano, B. J. et al. One-electron bonds in copper–aluminum and copper–gallium complexes. *Chem. Sci.* **13**, 6525–6531 (2022).
5. Ishigaki, Y., Shimajiri, T., Takeda, T., Katoono, R. & Suzuki, T. Longest C–C single bond among neutral hydrocarbons with a bond length beyond 1.8 Å. *Chem* **4**, 795–806 (2018).
6. Shimajiri, T. *The Nature of Ultralong C–C Bonds* (Springer Nature, 2023).
7. Pauling, L. The nature of the chemical bond. II. The one-electron bond and the three-electron bond. *J. Am. Chem. Soc.* **53**, 3225–3237 (1931).
8. Lewis, G. N. The atom and the molecule. *J. Am. Chem. Soc.* **38**, 762–785 (1916).
9. Langmuir, I. The arrangement of electrons in atoms and molecules. *J. Franklin Inst.* **187**, 359–362 (1919).
10. Clark, T. Odd-electron .sigma. bonds. *J. Am. Chem. Soc.* **110**, 1672–1678 (1988).
11. Ioffe, A. & Shaik, S. Ethane cation-radical isomers and their interconversion pathways. Electron shift isomerism in cation radicals. *J. Chem. Soc., Perkin Trans. 2* **3**, 1461 (1993).
12. Zuilhof, H., Dinnocenzo, J. P., Reddy, C. & Shaik, S. Comparative study of ethane and propane cation radicals by B3LYP density functional and high-level ab initio methods. *J. Phys. Chem.* **100**, 15774–15784 (1996).
13. de Sousa, D. W. O. & Nascimento, M. A. C. One-electron bonds are not 'half-bonds'. *Phys. Chem. Chem. Phys.* **21**, 13319–13336 (2019).
14. Claxton, T. A., Overill, R. E. & Symons, M. C. R. Possible structures for $C_2H_6^+$ and $B_2H_6^-$ E.S.R. evidence and UHF calculations. *Mol. Phys.* **27**, 701–706 (1974).
15. DuPont, T. J. & Mills, J. L. Arylborane anions. Electrochemical study. *J. Am. Chem. Soc.* **97**, 6375–6382 (1975).
16. Hudson, R. L. & Williams, F. Electron spin resonance spectrum of trimethyl borate ([(MeO)3B.cntdot.B(OMe)3]–). A novel .sigma. radical with a one-electron bond. *J. Am. Chem. Soc.* **99**, 7714–7716 (1977).
17. Kasai, P. H. & McLeod, D. Electron spin resonance study of molecular anions generated in argon matrix at 4°K: ESR spectrum of $B_2H_6^-$. *J. Chem. Phys.* **51**, 1250–1251 (1969).
18. Iwasaki, M., Toriyama, K. & Nunome, K. Electron spin resonance study of electronic and geometrical structures of $C_2H_6^+$ and other simple alkane cations at 4.2 K: possible evidence for Jahn–Teller distortion. *J. Am. Chem. Soc.* **103**, 3591–3592 (1981).
19. Wang, J. T. & Williams, F. E.S.R. spectra of the hexamethyldisilane and hexamethyldigermane radical cations. *J. Chem. Soc. Chem. Commun.* **1981**, 666–668 (1981).
20. Shida, T., Kubodera, H. & Egawa, Y. Confirmation of the cation radicals of hexamethylethane and hexamethyldisilane by ESR and other spectroscopy. *Chem. Phys. Lett.* **79**, 179–182 (1981).
21. Hoefelmeyer, J. D. & Gabbaï, F. P. An intramolecular boron–boron one-electron σ-bond. *J. Am. Chem. Soc.* **122**, 9054–9055 (2000).
22. Cataldo, L. et al. Formation of a phosphorus–phosphorus bond by successive one-electron reductions of a two-phosphinines-containing macrocycle: crystal structures, EPR, and DFT investigations. *J. Am. Chem. Soc.* **123**, 6654–6661 (2001).
23. Rao, V. R. & Hixson, S. S. Arylcyclopropane photochemistry. Electron-transfer-mediated photochemical addition of methanol to arylcyclopropanes. *J. Am. Chem. Soc.* **101**, 6458–6459 (1979).
24. Dinnocenzo, J. P., Todd, W. P., Simpson, T. R. & Gould, I. R. Nucleophilic cleavage of one-electron .sigma. bonds: stereochemistry and cleavage rates. *J. Am. Chem. Soc.* **112**, 2462–2464 (1990).
25. Miyashi, T., Ikeda, H., Konno, A., Okitsu, O. & Takahashi, Y. Photoinduced electron-transfer reactions of the cope and related systems. *Pure Appl. Chem.* **62**, 1531–1538 (1990).
26. Ikeda, H. et al. Photoinduced electron-transfer degenerate cope rearrangement of 2,5-diaryl-1,5-hexadienes: a cation-radical cyclization–diradical cleavage mechanism. *J. Am. Chem. Soc.* **120**, 87–95 (1998).
27. Ikeda, H. et al. Photoinduced electron-transfer cope rearrangements of 3,6-diaryl-2,6-octadienes and 2,5-diaryl-3,4-dimethyl-1,5-hexadienes: stereospecificity and an unexpected formation of the bicyclo[2.2.0]hexane derivatives. *J. Org. Chem.* **64**, 1640–1649 (1999).
28. Ikeda, H., Hoshi, Y. & Miyashi, T. 1,3-Bis(4-methoxyphenyl)cyclohexane-1,3-diyl cation radical: divergent reactivity depending upon electron-transfer conditions. *Tetrahedron Lett.* **42**, 8485–8488 (2001).
29. Gomberg, M. Triphenylmethyl, ein Fall von dreiwerthigem Kohlenstoff. *Ber. Dtsch. Chem. Ges.* **33**, 3150–3163 (1900).
30. Gomberg, M. An instance of trivalent carbon: triphenylmethyl. *J. Am. Chem. Soc.* **22**, 757–771 (1900).
31. Kahr, B., Van Engen, D. & Mislow, K. Length of the ethane bond in hexaphenylethane and its derivatives. *J. Am. Chem. Soc.* **108**, 8305–8307 (1986).
32. Takeda, T. et al. Hexaphenylethanes with an ultralong C–C bond: expandability of the C–C bond in highly strained tetraarylpyracenes. *Chem. Lett.* **42**, 954–962 (2013).
33. Suzuki, T. et al. Expandability of ultralong C–C bonds: largely different C1–C2 bond lengths determined by low-temperature X-ray structural analyses on pseudopolymorphs of 1,1-bis(4-fluorophenyl)-2,2-bis(4-methoxyphenyl)pyracene. *Chem. Lett.* **43**, 86–88 (2014).
34. Shimajiri, T., Suzuki, T. & Ishigaki, Y. Flexible C–C bonds: reversible expansion, contraction, formation, and scission of extremely elongated single bonds. *Angew. Chem. Int. Ed.* **59**, 22252–22257 (2020).
35. Dyker, G., Hagel, M., Henkel, G. & Köckerling, M. Naphthyl-substituted carbocations: from peri interaction to cyclization. *Eur. J. Org. Chem.* **2008**, 3095–3101 (2008).
36. Cordoneanu, A., Drewitt, M. J., Bavarian, N. & Baird, M. C. Synthesis and characterization of weakly coordinating anion salts of a new, stable carbocationic reagent, the dibenzosuberenyl (dibenzotropylium) ion. *New J. Chem.* **32**, 1890 (2008).
37. Nishiuchi, T. et al. Anthracene-attached persistent tricyclic aromatic hydrocarbon radicals. *Chem. Asian J.* **14**, 1830–1836 (2019).
38. Sun, D., Rosokha, S. V. & Kochi, J. K. Donor-acceptor (electronic) coupling in the precursor complex to organic electron transfer: intermolecular and intramolecular self-exchange between phenothiazine redox centers. *J. Am. Chem. Soc.* **126**, 1388–1401 (2004).
39. Small, D. et al. Intermolecular π-to-π bonding between stacked aromatic dyads. Experimental and theoretical binding energies and near-IR optical transitions for phenalenyl radical/radical versus radical/cation dimerizations. *J. Am. Chem. Soc.* **126**, 13850–13858 (2004).
40. Nojo, W., Ishigaki, Y., Takeda, T., Akutagawa, T. & Suzuki, T. Selective formation of a mixed-valence state from linearly bridged oligo(aromatic diamines): drastic structural change into a folded columnar stack for half-filled polycations. *Chem. Eur. J.* **25**, 7759–7765 (2019).
41. Casado, J. et al. Evidence for multicenter bonding in dianionic tetracyanoethylene dimers by Raman spectroscopy. *Angew. Chem. Int. Ed.* **52**, 6421–6425 (2013).
42. Kubo, T. et al. Long carbon-carbon bonding beyond 2 Å in Tris(9-fluorenylidene)methane. *J. Am. Chem. Soc.* **143**, 14360–14366 (2021).
43. Dutan, C. et al. Electron transfer between two silyl-substituted phenylene rings: EPR/ENDOR spectra, DFT calculations, and crystal structure of the one-electron reduction compound of a Di(m-silylphenylenedisiloxane). *J. Am. Chem. Soc.* **125**, 4487–4494 (2003).

# Methods

### General information

All commercially available compounds were used without further purification unless otherwise indicated. Acetonitrile was dried before use by distillation from $CaH_2$. Column chromatography was performed on silica gel (Wakogel 60N; neutral; particle size: 38–100 μm). $^1H$ and $^{13}C$ NMR spectra were recorded on a BRUKER AscendTM 400 ($^1H$/400 MHz and $^{13}C$/100 MHz) spectrometer. Mass spectra were recorded on a JEOL JMS-T100GCV spectrometer in FD mode (GC-MS&NMR Laboratory, Research Faculty of Agriculture, Hokkaido University). Melting points were measured on a Stanford Research Systems MPA100 Optimelt for powder samples and on a YANACO MP-J3 for single crystals; all values are uncorrected. The Raman spectroscopy using a 785 nm laser was carried out on a RENISHAW inVia Reflex at the OPEN FACILITY, Hokkaido University Sousei Hall. Infrared (IR) spectra were measured on a Shimadzu IRAffinity-1S spectrophotometer (attenuated total reflection (ATR) mode) for powder samples and on a JASCO IRT-5200FT/IR-6600 spectrophotometer for single crystals (Transmission Mode). X-band CW-EPR measurements were conducted using a Bruker BioSpin EMX Plus. Solid-state UV/Vis/NIR spectra were measured on a microscopic spectrometer (MSV 5200, JASCO; Transmission Mode), while solution-state UV/Vis/NIR spectra were recorded on a JASCO V-770 spectrophotometer.

DFT calculations were performed using the Gaussian 16W[44] program package. Parts of the DFT calculations for $\mathbf{1}^{\bullet+}$ were performed with the atomic coordinates obtained from the X-ray diffraction analysis of sample 1 of $\mathbf{1}^{\bullet+}I_3^-$ at 100 K. Multiwfn software[45] (v.3.8) was used for localized molecular orbital (Foster–Boys method) and topological analysis (quantum theory of atom in molecules and electron localized functions) of the electron density that was obtained from the DFT calculations. The NBO analyses were performed using v.3.1 of the NBO[46] function in the Gaussian 16W program package.

A suitable crystal was selected and used for the measurement on a Rigaku XtaLAB Synergy (Cu-Kα radiation, $\lambda = 1.54184$ Å) with HyPix diffractometer. Using Olex2 (ref. 47), the structure was solved with the SHELXT[48] structure solution program using Intrinsic Phasing and refined with the SHELXL[49] refinement package using least squares minimization.

### Starting material

HPE **1** was prepared according to literature procedures[5].

**Synthesis of radical cation salt $\mathbf{1}^{\bullet+}I_3^-$. 1** (4.74 mg, 8.93 μmol) was added to a solution of iodine (1.70 mg, 13.4 μmol) in dry $CH_2Cl_2$ (5 ml) at 26 °C. After stirring at 26 °C for 1 h, the resulting suspension was dried under reduced pressure to give a dark brown solid (6.4 mg). Mp: 157–163 °C (decomp.); $^1H$ NMR ($CD_3CN$): silent; IR (ATR): ν $cm^{-1}$ 3,046; 3,023; 1,607; 1,485; 1,465; 1,418; 1,310; 1,229; 1,164; 1,130; 1,111; 1077; 1,043; 952; 877; 863; 841; 825; 795; 767; 739; 723; 686; 672; 646; 627; 608; 587; 517; 485; 470; 430; 422; 420; LR-MS (FD) *m/z* (%): 532.26 (12), 531.26 (46), 530.25 ($M^+$, bp); HR-MS (FD) calculated for $C_{42}H_{26}$: 530.20345; Found: 530.20552.

Recrystallization of the obtained material from dry acetonitrile/dry tetrahydrofuran/dry diethyl ether gave dark violet crystals of $\mathbf{1}^{\bullet+}I_3^-$ (at least 0.06 mg, more than 1%), which were picked up with a needle and characterized by X-ray crystallography. The isolated yield was calculated based on the separated crystals from the as-prepared crystals, which might also contain **1**, $\mathbf{1}^{\bullet+}I_5^-$ (determined by preliminary X-ray analysis), and other forms of cationic species. Mp: 191–196 °C (decomp.); IR (a single crystal, transmission mode): ν $cm^{-1}$ 3,094; 3,045; 2,979; 2,925; 1,955; 1,929; 1,907; 1,819; 1,614; 1,587; 1,530; 1,455; 1,436; 1,345; 1,260; 1,207; 1,166; 1,149; 1,124; 1,084; 1,047; 947; 859; 839; 809; 777; 752; 725; 670; 611.

**Synthesis of dication salt $\mathbf{1}^{2+}(I_3^-)_2$. 1** (3.00 mg, 5.65 μmol) was added to a solution of iodine (2.15 mg, 16.9 μmol) in dry $CH_2Cl_2$ (5 ml) at 26 °C. After stirring at 26 °C for 1 h, the resulting suspension was dried under reduced pressure to give a dark violet solid (5.1 mg). Mp: 177–182 °C (decomp.); $^1H$ NMR ($CD_3CN$): silent (given that the reduction potential of iodine was not sufficient to oxidize radical cation $\mathbf{1}^{\bullet+}$ completely, the silent NMR spectrum was attributed to a partial contribution of radical cation $\mathbf{1}^{\bullet+}$.); IR (ATR): ν $cm^{-1}$ 3,042; 1,606; 1,529; 1,513; 1,476; 1,430; 1,419; 1,342; 1,318; 1,229; 1,189; 1,163; 1,128; 1,115; 1,088; 1,040; 990; 952; 941; 874; 859; 840; 811; 796; 774; 768; 751; 721; 711; 693; 676; 657; 627; 610; 551; 517; 469; LR-MS (FD) *m/z* (%): 532.18 (13), 531.18 (47), 530.17 ($M^+$, bp); HR-MS (FD) calculated for $C_{42}H_{26}$: 530.20345; Found: 530.20499.

Recrystallization of the obtained material from dry $CH_2Cl_2$/dry diethyl ether gave dark violet crystals of $\mathbf{1}^{2+}(I_3^-)_2$ (at least 0.10 mg, more than 2%), which were picked up with a needle and characterized by X-ray crystallography. The isolation yield was calculated based on the separated single crystals from the as-prepared crystals, which might contain $\mathbf{1}^{\bullet+}I_5^-$ (determined by preliminary X-ray analysis) or other cationic species.

Mp: 147–153 °C (decomp.); IR (a single crystal, transmission): ν $cm^{-1}$ 3,187; 3,078; 3,038; 2,928; 2,855; 1,907; 1,724; 1,646; 1,605; 1,514; 1,471; 1,440; 1,386; 1,358; 1,327; 1,256; 1,198; 1,121; 1,096; 991; 976; 941; 890; 866; 841; 793; 727; 661; 638.

## Data availability

The X-ray data have been deposited with the Cambridge Crystallographic Data Centre under reference numbers 2301032–2301035 ($\mathbf{1}^{\bullet+}I_3^-$, main_sample1), 2301036–2301039 ($\mathbf{1}^{\bullet+}I_3^-$, sub_sample2) and 2301040–2301043 ($\mathbf{1}^{2+}(I_3^-)_2$). All other data are presented in the main text or the Supplementary Information.


44. Frisch, J. M. et al. Gaussian 16, Revision C.01 (Gaussian, Inc., 2019).
45. Lu, T. & Chen, F. Multiwfn: a multifunctional wavefunction analyzer. *J. Comput. Chem.* **33**, 580–592 (2012).
46. Glendening, E. D., Reed, A. E., Carpenter, J. E. & Weinhold, F. NBO v.3.1 (Gaussian, Inc., 2001).
47. Dolomanov, O. V., Bourhis, L. J., Gildea, R. J., Howard, J. A. K. & Puschmann, H. OLEX2: a complete structure solution, refinement and analysis program. *J. Appl. Crystallogr.* **42**, 339–341 (2009).
48. Sheldrick, G. M. SHELXT – Integrated space-group and crystal-structure determination. *Acta Crystallogr. A Found. Adv.* **71**, 3–8 (2015).
49. Sheldrick, G. M. Crystal structure refinement with SHELXL. *Acta Crystallogr. C Struct. Chem.* **71**, 3–8 (2015).



**Acknowledgements** We thank E. Fukushi and Y. Takata (Hokkaido University) for recording mass spectra, H. Hirata (Hokkaido University) for recording electron spin resonance spectra, S. Noro, Y. Saito and A. Yamazaki for recording solid-state UV/Vis/NIR spectra, as well as J. P. Gong and T. Nakajima for recording solid-state IR spectra. Parts of the theoretical calculations were carried out at the Research Center for Computational Science, Okazaki, Japan (Project 23-IMS-C218). We would also like to thank U. F. J. Mayer at www.mayerscientificediting.com for proofreading our manuscript. This work was supported by the Masason Foundation (to S.K.) and by the Research Program 'Five-star Alliance' in 'NJRC Mater. & Dev.' of MEXT (Japan). Y. I. and T. Shimajiri acknowledge financial support from a Toyota Riken Scholarship. This work was furthermore supported by Grants-in-Aid from MEXT (JSPS Nos. 23K13726 to T. Shimajiri, 23K20275 to T. Suzuki, and 23K21107 and 23H04011 to Y.I.) and JST PRESTO (No. JPMJPR23Q1) to Y.I.


**Author contributions** T. Shimajiri, T. Suzuki and Y.I. developed the concept of this study. T. Shimajiri and S.K. conducted the synthetic and spectroscopic experiments as well as the theoretical calculations. T. Shimajiri, T. Suzuki and Y.I. supervised the project. T. Shimajiri prepared the manuscript with feedback from all authors.

**Competing interests** The authors declare no competing interests.

**Additional information**


**Supplementary information** The online version contains supplementary material available at https://doi.org/10.1038/s41586-024-07965-1.



**Correspondence and requests for materials** should be addressed to Takuya Shimajiri or Yusuke Ishigaki.



**Peer review information** *Nature* thanks Tobias Krämer and the other, anonymous, reviewer(s) for their contribution to the peer review of this work. Peer reviewer reports are available.